Vulnerability Identification and Evaluation of Interdependent Natural Gas-Electricity Systems

Lu Nan, *Student Member, IEEE*, Lei Wu, *Senior Member, IEEE*, Tianqi Liu, *Senior Member, IEEE*, Yikui Liu, *Student Member, IEEE*, and Chuan He, *Member, IEEE*

***Abstract*—The intensified interdependency of natural gas and electricity systems poses urgent needs and new challenges in identifying vulnerable components of the interdependent system, which could be significantly different from those of individual systems because of the interdependency. This paper proposes a method to identify and rank vulnerable components of interdependent natural gas-electricity systems. Specially, a topological model and the vulnerability index for the interdependent system are constructed, and vulnerable component identification method is put forward to select and rank components by simultaneously considering topological and functional vulnerabilities. The proposed vulnerable component identification method is quantitatively assessed via a security evaluation approach, which calculates electricity and gas supply-demand imbalance when the vulnerable components are out of service. Numerical results of a 6-bus electricity/7-node gas system and a modified IEEE 118-bus electricity/20-node gas system illustrate effectiveness of the proposed method.**

***Index Terms*—Interdependent infrastructures, graph theory, node contraction, vulnerability index, security evaluation.**

NOMENCLATURE

Variables with superscript b defined below correspond to the normal operation condition, and variables with superscript Δ used throughout the paper refer to their counterparts under contingency.

Parameters

$A_{g,i\to j}$, $A_{d,i\to j}$	Power transfer distribution factor of generator g/load d on line i-j
C_k^{gas}, C_s^{gas}	Production/storage cost of gas well k/storage s
C_g^{fuel}	Fuel price of generator g
e_c^{com}	Efficiency of compressor c
E_s^{min}, E_s^{max}	Min/max volume of gas storage s
F_g^c	Fuel consumption of generator g
G_k^{min}, G_k^{max}	Min/max production capacity of gas well k
$G_{w,t}^b$	Gas consumption of gas load w at time t
HHV	Higher heating value
$K_{g,i\to j}$, $K_{d,i\to j}$	Generalized power transfer distribution factor of generator g/load d on line i-j
K_{mn}	Gas flow constant of pipeline m-n
L_{mn}	Linepack constant of pipeline m-n
$P_d^{\sim}$	Electricity demand of load d
$P_{d,t}^b$	Electricity supply to electrical load d at time t
$P_g^{\sim}$	Generation output of generator g
$P_{i\to j}^{\sim}$	Power flow of line i-j
$P_{ij}^{\sim}$	Gas flow of pipeline i-j
P_g^{min}, P_g^{max}	Min/max capacity of generator g
PL_l^{max}	Maximum power flow limit of line l
Q_s^{min}, Q_s^{max}	Min/max inflow and outflow of gas storage s
R_g^{down}, R_g^{up}	Down/up corrective capability of generator g
SU_g, SD_g	Constant start-up/shutdown cost of generator g
T_g^{on}, T_g^{off}	Min ON/OFF time limit of generator g
UR_g, DR_g	Ramp up/down rate of generator g
x_l	Reactance of transmission line l
θ_e^{min}, θ_e^{max}	Min/max bus voltage phase angle of bus e
π_m^{min}, π_m^{max}	Min/max squared pressure of gas node m
τ_c	Compressor factor of gas compressor c
Φ	Energy conversion factor.

Variables

$C_L(i)$	Local centrality of vertex i
$E_{s,t}^b$	Volume of gas storage s at time t
$E_{mn,t}^b$	Linepack of pipeline m-n at time t
$G_{g,t}^b$	Gas consumption of gas-fired unit g at time t
$G_{k,t}^b$	Production of gas well k at time t
$GL_{mn,t}^b$	Gas flow of pipeline m-n at time t
$I_{g,t}^b$	Unit commitment status of generator g at time t
$N(p)$	Number of the nearest and the second nearest neighbors of p
$P_{d,i\to j}$, $P_{g,i\to j}$	Component of power fl on line i-j delivered to load d/ supplied by generator g
$P_{c,t}^b$	Electricity consumption of compressor c at time t
$P_{g,t}^b$	Dispatch of generator g at time t
$PL_{l,t}^b$	Power flow of line l at time t

Manuscript received September 14, 2019; revised January 2, 2020; accepted January 16, 2020. Date of publication January 21, 2020; date of current version June 19, 2020. This work was supported in part by the U.S. National Science Foundation under Grant CNS-1915756 and Grant CMMI-1906780, and in part by the Fundamental Research Funds for the China Central Universities under Grant YJ201859. Paper no. TSG-01361-2019. *(Corresponding author: Lei Wu.)*

Lu Nan, Tianqi Liu, and Chuan He are with the College of Electrical Engineering, Sichuan University, Chengdu 610065, China.

Lei Wu and Yikui Liu are with the ECE Department, Stevens Institute of Technology, Hoboken, NJ 07901 USA (e-mail: lei.wu@stevens.edu).

Color versions of one or more of the figures in this article are available online at http://ieeexplore.ieee.org.

Digital Object Identifier 10.1109/TSG.2020.2968178

$Q^{in,b}_{s,t}$, $Q^{out,b}_{s,t}$	Inflow/outflow of gas storage s at time t
$Q^{in,b}_{mn,t}$, $Q^{out,b}_{mn,t}$	Inflow/outflow of pipeline m-n at time t
$Q^{b}_{c,t}$	Gas flow of compressor c at time t
$su^{b}_{g,t}$, $sd^{b}_{g,t}$	Start-up/shutdown cost of generator g at time t
wf^{e}_{ij}, wf^{g}_{ij}	Flow weight of transmission line i-j/pipeline i-j
wt_{ij}	Topology weight of line i-j
WF^{e}_{i}, WF^{g}_{i}	Flow vulnerability index of electricity/gas component i
WT_i	Topology vulnerability index of component i
$X^{on}_{g,t}$, $X^{off}_{g,t}$	ON/OFF time counter of generator g at time t
z_r	Filling condition
$\theta^{b}_{e,t}$	Voltage phase angle of bus e at time t
$\theta^{b}_{s(l),t}$, $\theta^{b}_{r(l),t}$	Sending/receiving bus phase angle of line l at time t
$\pi^{b}_{m,t}$	Squared pressure of gas node m at time t
$\rho_{m,t}$	Pressure of gas node m at time t
$\rho^{b}_{mn,t}$	Average pressure of gas nodes m and n at time t
δ_r	Segment value for interval r.

Sets and Indices

d, e, g, l, t	Indices for electrical loads, buses, generators, lines, and hours
c, f, k, mn, s, w	Indices for gas compressors, nodes, supplies, pipelines, storage facilities, and loads
i, j, p, q, m, n	Indices for vertices/gas network nodes
$s(l)$, $r(l)$	Sending/receiving bus of electrical line l
$\mathcal{D}, \mathcal{E}, \mathcal{G}, \mathcal{L}, \mathcal{T}$	Sets of electrical loads, buses, generators, lines, and hours
$\mathcal{F}, \mathcal{K}, \mathcal{W}$	Sets of gas nodes, supplies, and loads
$\mathcal{C}, MN, \mathcal{S}, \mathcal{GU}$	Set of gas compressors, pipelines, storage facilities, and gas-fired generators
$G(f)$, $N(e)$	Set of network components connected at gas node f/electrical bus e
$\Gamma(i)$	Set of the nearest neighbors of vertex i
$\beth$	Set of contingencies.

I. Introduction

THE MODERN society is becoming increasingly relying on the interconnected and interdependent critical infrastructures, such as nexus of electricity-water-wastewater [1], electricity-telecom-water [2], and natural gas-electricity [3], to support the security, economic prosperity, and social well-being. Indeed, in the U.S., the natural gas system is playing an increasingly important role to the power system, because of its direct impacts on unit commitment and dispatch of gas-fired generators and consequently on the operational economics and reliability of the power grid. According to the U.S. Energy Information Administration and the U.S. Department of Energy, natural gas consumption for electricity generation has increased 30.44% in 2018 compared to 2014 [4].

Since the natural gas system is highly intertwined with the power grid, any disturbance or failure on one infrastructure may propagate to the other one and cause disruption. To this end, the interdependent system may fail not only because of their individual complexities, but also because of their tight interdependence. The greater the interdependence between the two systems, the more vulnerable the overall interdependent system. Coordinated operation of natural gas and electricity systems has been analyzed recently [5]–[8]. References [5] and [6] proposed robust co-optimization models to analyze the coordinated short-term scheduling and long-term planning of electricity and gas systems. The transient characteristics of gas flow was considered in [7] when modeling short-term coordinated scheduling of the interdependent electricity and natural gas infrastructures. Reference [8] studied effects of natural gas system failures on the integrated natural gas and electricity systems, and analyzed predictive control actions to mitigate the impact of failures. Indeed, existing research works described above employed different approaches to focus on the simulation, operation, planning, and reliability quantification of the interdependent infrastructures, while analysis on system vulnerability is very limited.

In this paper, to analyze vulnerability of interdependent infrastructures, we define vulnerable components as the ones that will severely compromise security performance when out of service. Empirical approach, agent-based approach, system dynamic-based approach, economic theory-based approach, and network-based approach are the five generally used methods to identify vulnerable components [9]. Network-based approach is a widely used method for the interdependent natural gas-electricity system, which can be further classified as topological method [3], [10]–[15] and functional method [16]–[18] based on the level of system details adopted to simulate infrastructures. Specifically, topological vulnerability analysis only needs infrastructure topological information, while functional vulnerability analysis also needs system operation mechanisms. Reference [3] analyzed both topological vulnerability and functional vulnerability by using infrastructure topologies and operating regimes. Topological vulnerability analysis is used to enhance infrastructures in the long-term planning, and functional vulnerability analysis is used to protect infrastructures in the short-term operation. Reference [10] proposed an index based on graph theory to analyze topological vulnerability of the integrated electricity and natural gas systems. In reference [11], the geodesic vulnerability index was used to access vulnerability of interdependent electricity and natural gas infrastructures, which has also been widely used to evaluate vulnerability of the power grid [12], [13]. Reference [14] used nodal degree, average shortest length, and geodesic vulnerability index to assess topological vulnerability of the interdependent natural gas and electricity transmission network for expansion planning. However, using pure topological metrics to analyze interdependence can lead to misleading results that cannot allocate resources effectively to mitigate risks [15].

On the other hand, functional method [16]–[18] can identify critical physical components more accurately by capturing flow characteristics of interdependent systems.

Reference [16] proposed an integrated simulation model to analyze interdependent natural gas-electricity systems, which considers gas dependency of gas-fired power plants and electrical dependency of electric-driven gas compressors. In reference [17], a vulnerability index was put forward to analyze the mechanism of fault propagation of power systems based on complex network theory. Reference [18] developed a vulnerability assessment tool according to artificial neural network which can be used for real-time applications. However, computational cost of the functional method could be high when detailed operation mechanisms are modeled.

In observing distinct limitations of individual methods, this paper targets to develop an approach that simultaneously considers topological and functional characteristics to effectively identify vulnerable components of the interdependent natural gas-electricity system. In particular, we construct a topological model of the interdependent natural gas-electricity system, and propose a novel vulnerability index by integrating both topological and functional vulnerabilities to identify vulnerable components of the interdependent system. A co-optimization model is adopted to accurately access functional characteristics of the interdependent system under optimal operation condition, and a security evaluation method is constructed to quantify the impacts of the identified vulnerable components by calculating electricity and gas supply-demand imbalance.

The main contributions are summarized as follows:

(i) Unlike traditional methods that only model buses and transmission lines in the power grid as well as gas nodes, compressors, and pipelines in the natural gas system, we construct a detailed topological model to describe topology of the interdependent natural gas-electricity system with additional valuable information: (1) generators and loads of the power grid; (2) gas storage facilities, supplies, and loads of the gas system; (3) connections between gas-fired units and gas nodes as well as between electric-driven compressors and electricity buses. The detailed topological model is further refined based on node contraction theory [19] to reduce the scale of the topological model while preserving original features of the detailed model;

(ii) The proposed vulnerability index simultaneously considers topological and functional characteristics of the interdependent system to effectively identify vulnerable components. Moreover, the proposed approach can select vulnerable components dynamically with respect to various operation conditions;

(iii) The security evaluation method is proposed to quantify impacts on the interdependent system when vulnerable components are out of service. Electricity and gas supply-demand imbalance is calculated under contingency condition, while considering both gas dependency of the power system and electrical dependency of the natural gas system.

The remainder of this paper is organized as follows: Section II describes the topological model of the interdependent natural gas-electricity system. Section III details topological and functional vulnerabilities of the interdependent system and presents the vulnerability identification approach. Section IV builds the co-optimization model for the interdependent system to assess functional characteristics, and discusses a security evaluation model to quantify the selected vulnerable components. Section V verifies effectiveness of the proposed approach via several test systems, and conclusions are drawn in Section VI.

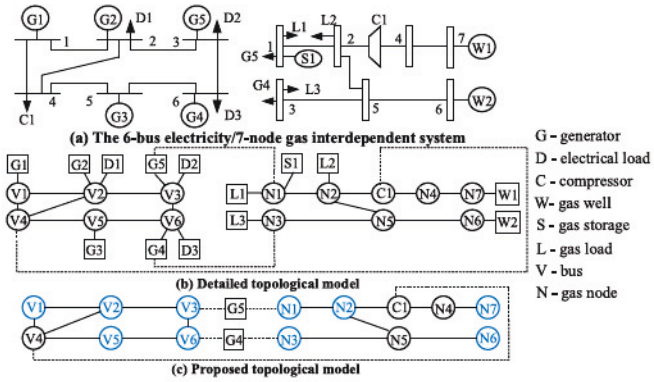

Fig. 1. Topological model of a 6-bus electricity/7-node gas interdependent system.

II. Topological Model of the Interdependent System

The interdependent natural gas-electricity system can be described as a graph with sets of vertices and edges: each vertex represents a component in the interdependent system, and each edge represents a link between components. In this section, a 6-bus electricity/7-node gas interdependent system as shown in Fig. 1 is used to facilitate the discussion of the proposed topological model.

As shown in Fig. 1(a), the 6-bus system includes three non-gas thermal units G1-G3, two gas-fired units G4-G5, three electrical loads D1-D3, one electric-driven gas compressor load, and seven transmission lines. The 7-node gas system includes two gas wells W1-W2, one gas storage S1, one compressor C1, three gas loads L1-L3, two gas-fired thermal unit loads, and six pipelines. Three interdependencies between the two systems are considered: gas dependency of gas-fired unit G4, gas dependency of gas-fired unit G5, and electrical dependency of electric-driven gas compressor C1.

In the traditional topological models [20]–[21], substations of power systems are often represented as vertices while transmission lines and transformers are represented as edges. However, components connected to substations, i.e., generators, loads, and reactive power compensators are disregarded [20]. Similarly, gas nodes and compressors of the gas systems consist of vertices, and pipelines are represented as edges, while gas wells, gas loads, and gas storage are not explicitly included [21]. Therefore, traditional topological models are incomplete and lack certain important infrastructure details.

A more detailed topological model is shown in Fig. 1(b), which accurately captures interdependency of natural gas and electricity systems induced by physical components, i.e., gas-fired generators and gas compressors. For instance, Fig. 1(b) clearly shows that a disconnection of dependency G5-N1 will directly impact only G5, instead of the entire bus V3 in the traditional topological model. Thus, the detailed topological model makes it possible to accurately identify and rank vulnerable components via distinct topological importance.

Although the detailed topological model provides a more accurate representation of interdependent natural gas-electricity system that is more appropriate to identify vulnerable infrastructures, the increased number of vertices and edges could induce high computational burden. For this reason, we use node contraction theory [19] to refine the proposed sophisticated topological model and reduce scale of the detailed topological model while preserving all characteristic details.

In a graph with weight of each vertex being 1, the degree of each vertex is defined as the number of adjacent vertices [22], [23]. For example, in Fig. 1(b), degrees of G1 and V1 are 1 and 3, respectively. We apply node contraction to merge degree-1 vertices to its connecting vertices, and modify weights of remaining vertices accordingly. As shown in Fig. 1(c), G1 is merged to V1, and the weight and the degree of V1 are both modified as 2.

Indeed, in the interdependent natural gas-electricity system, vertices merged through the node contraction process can be electrical loads, gas loads, gas storages, gas wells, and non-gas thermal units, while their physical characteristics can be fully preserved at the original connecting vertices. Specifically, (i) with respect to the topological feature, the vertex being removed only connects to one vertex, thus whenever it is involved, its connecting vertex will also be involved; (ii) in terms of the functional feature, flow of the line between the merged vertex and the removed original vertex is always solely injected into/withdrawn from the merged vertex, which can be fully represented at the merged vertex. Therefore, a vertex with degree value of 1 can be merged to its original connecting vertex to refine the topological model and further reduce scale of the topological model. The advantages of such representations will be illustrated via numerical studies, which have not been fully studied in literature.

III. Vulnerable Component Identification in Interdependent Natural Gas-Electricity System

In graph theory, degree centrality [23], betweenness centrality [24], closeness centrality [25], and local centrality [26] are widely used to select and rank vulnerable components of networked systems. A promising advantage of these approaches is their computational efficiency. However, these indicators only consider topological vulnerability while neglecting important functional characteristics, such as physical flow patterns. To this end, topological vulnerability analysis may not derive reliable results that necessarily reflect true vulnerabilities of components.

In this section, the concept of local centrality in graph theory and physical flow pattern characteristics of the interdependent natural gas-electricity system are considered together to derive vulnerability index, which can dynamically identify vulnerable components based on topological and functional characteristics simultaneously.

A. Vulnerability Index

According to degree centrality [23], in the interdependent natural gas-electricity system, components with higher degrees are likely to be more vulnerable. That is, if a component with higher degree is compromised, its failure may spread more quickly with more intensive impacts. However, this approach may fail in certain occasions because it only considers limited information of component's neighbors. On the other hand, betweenness centrality [24] and closeness centrality [25] consider global information of the graph, and can better quantify vulnerability of components with higher computational complexity. To this end, local centrality [26] is used in this paper as a trade-off between accuracy and computational complexity to identify vulnerable components of the interdependent natural gas-electricity system.

To make the vulnerability identification method more effective, physical flow pattern characteristics are also considered. In recognizing that characteristics and magnitudes of power flows and gas flows are significantly different, physical flow pattern characteristics of electricity and natural gas systems will be quantified individually, and combined after normalization to identify vulnerable components.

The vulnerability index R is defined as in (1), considering both topological vulnerability WT_i and functional vulnerability WF_i of the interdependent system. Specifically, topological vulnerability WT_i of component i, defined as in (2), is topological weighted sum of edges connecting the component; functional vulnerability WF_i of component i is flow weighted sum of edges connecting the component, defined as WF_i^e in (3) for electricity grid and WF_i^g in (4) for natural gas system. For the interdependent natural gas-electricity system, topological weight wt_{ij} of line i-j is quantified via local centrality as in (5), which considers both the nearest and the second nearest neighbors of the component. According to Section II, because the node contraction theory is adopted, the merged degree-1 vertices are also included when calculating local centrality, while the methods to calculate topological weights of weight-1 vertices and other vertices are slightly different. For the power system, flow weight wf_{ij}^e is assessed by active power flow exchange between the pair of generator-load vertices carried by line i-j, calculated as in (6)-(7). That is, $K_{g,i\to j}$ is generation coefficient of generator g on line i-j [27], and $P_{g,i\to j}$ is active power flow component of line i-j supplied by generator g. Similarly, $P_{d,i\to j}$ is active power flow component of line i-j delivered to load d. Consequently, $|P_{g,i\to j}\cdot P_{d,i\to j}/P_{i\to j}^{\sim}|$ is active power flow exchange between generator g and load d carried on line i-j. The greater the contribution of a line to power flow exchange between generator-load vertex pairs, the more vulnerable if that line is lost. For natural gas system, flow weight wf_{ij}^g is represented by gas flow of line i-j. It is worthwhile to mention that values of power flow and gas flow used in (3)-(4) are obtained from the co-optimization scheduling of interdependent natural gas-electricity system which will be detailed in Section IV. For degree-1 vertices merged via the node contraction theory, flow of a line between the merged degree-1 vertex and its original connecting vertex can be represented by the flow injection/withdraw of the merged degree-1 vertex.

$$R_i = WT_i \cdot WF_i \tag{1}$$

$$WT_i = \sum_{j\in\Gamma(i)} wt_{ij} \tag{2}$$

$$WF_i^e = \sum_{j\in\Gamma(i)} wf_{ij}^e;\ wf_{ij}^e = \sum_{g\in\mathcal{G}}\sum_{d\in\mathcal{D}} \left| \frac{P_{g,i\to j}\cdot P_{d,i\to j}}{P_{i\to j}^{\sim}} \right| \quad (3)$$

$$WF_i^g = \sum_{j\in\Gamma(i)} wf_{ij}^g;\ wf_{ij}^g = \left| P_{ij}^{\sim} \right| \quad (4)$$

$$wt_{ij} = C_L(i)\times C_L(j);\ C_L(i) = \sum_{q\in\Gamma(i)}\sum_{p\in\Gamma(q)} N(p) \quad (5)$$

$$P_{g,i\to j} = K_{g,i\to j}\cdot P_g^{\sim};\ P_{d,i\to j} = K_{d,i\to j}\cdot P_d^{\sim} \quad (6)$$

$$K_{g,i\to j} = A_{g,i\to j} + \frac{P_{i\to j}^{\sim} - \sum_{g'\in(\mathcal{G}-1)} A_{g',i\to j} P_{g'}}{\sum_{g''\in\mathcal{G}} P_{g''}};$$

$$K_{d,i\to j} = A_{d,i\to j} + \frac{P_{i\to j}^{\sim} - \sum_{d'\in(\mathcal{D}-1)} A_{d',i\to j} P_{d'}}{\sum_{d''\in\mathcal{D}} P_{d''}};$$

$$g', d' \neq \text{reference bus.} \quad (7)$$

In summary, WT_i describes topological vulnerability via local centrality, while WF_i further represents functional vulnerability according to physical flow pattern characteristics. Therefore, vulnerability index R_i could reasonably quantify vulnerabilities of components in the interdependent natural gas-electricity system. In addition, because topology of the interdependent system, output of generators, as well as power flow and gas flow patterns could change dynamically against different operation conditions, values of R_i for individual components would also be different. Thus, R_i represents a dynamic vulnerability index which changes under different operation conditions.

B. Vulnerable Component Identification Procedure

Based on the above vulnerability index, the procedure for identifying vulnerable components of interdependent natural gas-electricity system is summarized as follows:

(i) Describes detailed topological model of the interdependent system and refine the topological model based on node contraction theory according to Section II;

(ii) Calculate vulnerability indices for individual components:
  (a) Conduct the co-optimization scheduling of interdependent system to derive optimal generation dispatch as well as power flows and gas flows;
  (b) Calculate topological vulnerability for each component as in (2);
  (c) Calculate functional vulnerability of power system components via (3) and gas system components via (4);
  (d) Normalize the value of topological and functional vulnerabilities, and calculate vulnerability index R_i.

(iii) Rank components based on vulnerability index values;

(iv) Choose a reasonable approach to quantify effects of vulnerable components failures.

IV. Co-Optimization Model of Interdependent Natural Gas-Electricity System and the Security Evaluation

The co-optimization model of interdependent natural gas-electricity system is discussed in this section. Moreover, a security evaluation approach is proposed to quantify impacts of vulnerable components failures on the interdependent system. The co-optimization and security evaluation models developed in this section are both mixed-integer linear programing (MILP) problems. Two types of dependencies are considered in the models: gas dependency of gas-fired units and electrical dependency of electric-driven compressors, while only the former is studied in most literature. The degree-1 vertices to be merged are always non-gas thermal units, electrical loads, gas loads, gas storages, or gas wells. In addition, the calculation of power/gas flow of the line between the degree-1 vertex to be merged and its connecting vertex is not needed, which can be directly represented by the energy generation/consumption of the degree-1 vertex. Moreover, the calculation of nodal energy balance is not needed for the degree-1 vertices to be merged.

A. Co-Optimization Model

As discussed in Section III-B, the MILP based co-optimization model is developed to derive optimal generation dispatch and functional characteristics of the interdependent natural gas and electricity system. Outputs of generators, power flow of transmission lines, and gas flow of pipelines obtained from the co-optimization model are used to calculate functional vulnerabilities of components.

• *Objective:* The objective of the co-optimization model is to minimize the normal operation cost of interdependent natural gas-electricity system (8), including production costs and startup/shutdown costs of non-gas thermal units, gas production costs, and gas storage costs.

$$\min \sum_{t\in\mathcal{T}} \left\{ \begin{array}{l} \sum\limits_{g\notin\mathcal{GU}} C_g^{fuel}\cdot\left[F_g^c\left(P_{g,t}^b\right)\cdot I_{g,t}^b + su_{g,t}^b + sd_{g,t}^b\right] \\ + \sum\limits_{k\in\mathcal{K}}\left(C_k^{gas}\cdot G_{k,t}\right) + \sum\limits_{s\in\mathcal{S}}\left(C_s^{gas}\cdot Q_{s,t}^{out,b}\right) \end{array} \right\}. \quad (8)$$

• *Constraints for Power System:* Power system constraints include operation limits of individual generators (9)-(15) and network constraints (16)-(19). Operation limits of individual generators include capacity limits (9), ramp up and ramp down limits (10)-(11), minimum ON/OFF time limits (12)-(13), as well as startup and shutdown costs limits (14)-(15). Network constraints include nodal balance limits (16) and transmission capacity limits (17). In this paper, DC power flow model is used to calculate power flows of transmission lines (18)-(19), while transmission losses is not included. $\theta_{ref,t}^b$ in (19) is voltage phase angle of the reference bus. It is noteworthy that transmission losses could be considered in the co-optimization model, by constructing the DC power flow model with losses [28] and further linearizing it by Taylor expansion [29] to consider energy losses. The renewable energy production as well as its uncertainties are not included in the co-optimization model, which can be incorporated by extending the proposed model into a stochastic or robust optimization framework [5], [30], [31]. Indeed, flexibilities of the interdependent natural gas-electricity system, such as fast response capabilities of gas-fired units, storage capabilities of gas storage and linepack in

pipelines, as well as energy conversion capabilities of Power to gas (P2G), could be used to effectively mitigate uncertainties of renewable energy production.

$$P_g^{min} \cdot I_{g,t}^b \le P_{g,t}^b \le P_g^{max} \cdot I_{g,t}^b; \qquad g \in \mathcal{G}, t \in \mathcal{T} \tag{9}$$

$$P_{g,t}^b - P_{g,(t-1)}^b \le UR_g \cdot I_{g,(t-1)}^b + P_g^{min} \cdot \left(I_{g,t}^b - I_{g,(t-1)}^b\right) + P_g^{max} \cdot \left(1 - I_{g,t}^b\right); \qquad g \in \mathcal{G}, t \in \mathcal{T} \tag{10}$$

$$P_{g,(t-1)}^b - P_{g,t}^b \le DR_g \cdot I_{g,t}^b + P_g^{min} \cdot \left(I_{g,(t-1)}^b - I_{g,t}^b\right) + P_g^{max} \cdot \left(1 - I_{g,(t-1)}^b\right); \qquad g \in \mathcal{G}, t \in \mathcal{T} \tag{11}$$

$$\left(X_{g,(t-1)}^{on} - T_g^{on}\right) \cdot \left(I_{g,(t-1)}^b - I_{g,t}^b\right) \ge 0; \qquad g \in \mathcal{G}, t \in \mathcal{T} \tag{12}$$

$$\left(X_{g,(t-1)}^{off} - T_g^{off}\right) \cdot \left(I_{g,t}^b - I_{g,(t-1)}^b\right) \ge 0; \qquad g \in \mathcal{G}, t \in \mathcal{T} \tag{13}$$

$$su_{g,t}^b \ge SU_g \cdot \left(I_{g,t}^b - I_{g,(t-1)}^b\right); \ su_{g,t}^b \ge 0; \qquad g \in \mathcal{G}, t \in \mathcal{T} \tag{14}$$

$$sd_{g,t}^b \ge SD_g \cdot \left(I_{g,(t-1)}^b - I_{g,t}^b\right); \ sd_{g,t}^b \ge 0; \qquad g \in \mathcal{G}, t \in \mathcal{T} \tag{15}$$

$$\sum_{g \in N(e) \cap \mathcal{G}} P_{g,t}^b - \sum_{s(l) \in N(e) \cap \mathcal{L}} PL_{l,t}^b + \sum_{r(l) \in N(e) \cap \mathcal{L}} PL_{l,t}^b = \sum_{d \in N(e) \cap \mathcal{D}} P_{d,t}^b + \sum_{c \in N(e) \cap \mathcal{C}} P_{c,t}^b; \qquad e \in \mathcal{E}, t \in \mathcal{T} \tag{16}$$

$$-PL_l^{max} \le PL_{l,t}^b \le PL_l^{max}; \qquad l \in \mathcal{L}, t \in \mathcal{T} \tag{17}$$

$$PL_{l,t}^b = \left[\theta_{s(l),t}^b - \theta_{r(l),t}^b\right] / x_l; \qquad l \in \mathcal{L}, t \in \mathcal{T} \tag{18}$$

$$\theta_e^{min} \le \theta_{e,t}^b \le \theta_e^{max}; \ \theta_{ref,t}^b = 0; \qquad e \in \mathcal{E}, t \in \mathcal{T}. \tag{19}$$

• *Constraints for Natural Gas System:* Natural gas system constraints include gas supply capacity limits (20), gas storage capacity limits (21)-(22), gas storage injection/withdrawal rate limits (23)-(24), nodal balance limits (25), gas flow calculation (26)-(27), and gas nodal pressure limits (28). The relationship of the two nodal pressures for a pipeline with compressor is modeled as in (29). Linepack represents the natural gas quantity contained in the pipeline, which is described as in (30)-(33). L_{mn} in (30) is a constant depending on characteristics of pipelines. Natural gas consumption of gas-fired units is calculated as in (34). As the detailed electricity consumption model of electric-driven gas compressors is nonlinear [32]–[34] with high computational complexity, in this paper, the simplified linear model (35) [35] is used to calculate electricity consumption of electric-driven gas compressors with favorable computation efficiency. *HHV* (with unit of MMBtu/kcf) and Φ (with unit of MMBtu/MWh) are used in (35) to convert energy quantities from kcf to MW.

In this paper, the relationship between nodal pressures and pipeline gas flow rates is modeled via the nonlinear equations (26)-(27), in which K_{mn} is a constant depending on characteristics of pipelines [36]. Nonlinear equations (26)-(27) can be linearized using the big M theory [5] and the piecewise linear approximation method [37]. Specifically, the non-linear equations (26)-(27) can be rewritten as in (36), and further reformulated as in (37) by employing big-M method with additional binaries $f_{mn,t}^+$ and $f_{mn,t}^-$ to indicate gas flow directions. $f_{mn,t}^+ = 1$ represents that gas flow in pipeline m-n is from m to n, while $f_{mn,t}^- = 1$ indicates the opposite flow direction. The bilinear $(\pi_{m,t}^b - \pi_{n,t}^b) \cdot (f_{mn,t}^+ - f_{mn,t}^-)$ in (36) can be equivalently reformulated as in (38) according to [38]. The quadratic term $y = GL_{mn,t}^{b2}$ in (36) can be piecewise linearized as in (39) [37]. The quadratic term $\pi_{m,t}^b = \rho_{m,t}^{b2}$ in (31) can also be linearized via the piecewise linear approximation method [37]. Consequently, the non-linear gas flow equation is converted into a MILP model. It is noteworthy that, proper values of M and the number of segments in the linear approximation process should be set to leverage computation efficiency and accuracy [37], [39].

$$G_k^{min} \le G_{k,t}^b \le G_k^{max}; \qquad k \in \mathcal{K}, t \in \mathcal{T} \tag{20}$$

$$E_{s,t}^b = E_{s,(t-1)}^b + Q_{s,t}^{in,b} - Q_{s,t}^{out,b}; \qquad s \in \mathcal{S}, t \in \mathcal{T} \tag{21}$$

$$E_s^{min} \le E_{s,t}^b \le E_s^{max}; \qquad s \in \mathcal{S}, t \in \mathcal{T} \tag{22}$$

$$Q_s^{min} \le Q_{s,t}^{in,b} \le Q_s^{max}; \qquad s \in \mathcal{S}, t \in \mathcal{T} \tag{23}$$

$$Q_s^{min} \le Q_{s,t}^{out,b} \le Q_s^{max}; \qquad s \in \mathcal{S}, t \in \mathcal{T} \tag{24}$$

$$\sum_{k \in G(f) \bigcap \mathcal{K}} G_{k,t}^b + \sum_{s \in G(f) \bigcap \mathcal{S}} \left(Q_{s,t}^{out,b} - Q_{s,t}^{in,b}\right) + \sum_{mn \in G(f) \bigcap MN} \left(Q_{mn,t}^{out,b} - Q_{mn,t}^{in,b}\right) = \sum_{g \in G(f) \bigcap \mathcal{G}} G_{g,t}^b + \sum_{w \in G(f) \bigcap \mathcal{W}} G_{w,t}^b; \qquad f \in \mathcal{F}, t \in \mathcal{T} \tag{25}$$

$$GL_{mn,t}^b = \mathrm{sgn}\left(\pi_{m,t}^b, \pi_{n,t}^b\right) \cdot K_{mn} \cdot \sqrt{\left|\pi_{m,t}^b - \pi_{n,t}^b\right|}; \qquad t \in \mathcal{T}, m, n \in \mathcal{F}, mn \in MN \tag{26}$$

$$\mathrm{sgn}\left(\pi_{m,t}^b, \pi_{n,t}^b\right) = \begin{cases} 1, & \pi_{m,t}^b \ge \pi_{n,t}^b \\ -1, & \pi_{m,t}^b < \pi_{n,t}^b \end{cases}; \qquad m, n \in \mathcal{F}, t \in \mathcal{T} \tag{27}$$

$$\pi_m^{min} \le \pi_{m,t}^b \le \pi_m^{max}; \qquad m \in \mathcal{F}, t \in \mathcal{T} \tag{28}$$

$$\pi_{m,t}^b \le \tau_c^2 \cdot \pi_{n,t}^b; \qquad m, n \in \mathcal{F}, t \in \mathcal{T} \tag{29}$$

$$E_{mn,t}^b = L_{mn} \cdot \rho_{mn,t}^b; \qquad mn \in MN, \ t \in \mathcal{T} \tag{30}$$

$$\rho_{mn,t}^b = \left(p_{m,t}^b + p_{n,t}^b\right)/2; \ \pi_{m,t}^b = \rho_{m,t}^{b\ 2}; \qquad m, n \in \mathcal{F}, \ t \in \mathcal{T} \tag{31}$$

$$E_{mn,t}^b = E_{mn,(t-1)}^b + Q_{mn,t}^{in,b} - Q_{mn,t}^{out,b}; \qquad mn \in MN, \ t \in \mathcal{T} \tag{32}$$

$$GL^b_{mn,t} = \left(Q^{in,b}_{mn,t} + Q^{out,b}_{mn,t}\right)/2; \qquad mn \in MN,\ t \in \mathcal{T} \quad (33)$$

$$G^b_{g,t} = \frac{\left[\left(F^c_g\left(P^b_{g,t}\right)\cdot I^b_{g,t}\right) + su^b_{g,t} + sd^b_{g,t}\right]}{\text{HHV}}; \qquad g \in \mathcal{GU}, t \in \mathcal{T} \quad (34)$$

$$P^b_{c,t} = \left(1 - e^{com}_c\right)\cdot Q^b_{c,t}\cdot \text{HHV}/\Phi; \qquad c \in \mathcal{C},\ t \in \mathcal{T} \quad (35)$$

$$GL^{b\ 2}_{mn,t} = K_{mn}{}^2 \cdot \left(\pi^b_{m,t} - \pi^b_{n,t}\right)\cdot\left(f^+_{mn,t} - f^-_{mn,t}\right); \quad t \in \mathcal{T}, m, n \in \mathcal{F}, mn \in MN \quad (36)$$

$$\begin{cases} \left(f^+_{mn,t} - 1\right)\cdot M = GL_{mn,t} = \left(1 - f^-_{mn,t}\right)\cdot M \\ \left(f^+_{mn,t} - 1\right)\cdot M = \pi_{m,t} - \pi_{n,t} = \left(1 - f^-_{mn,t}\right)\cdot M \\ f^+_{mn,t} + f^-_{mn,t} = 1 \end{cases} \quad t \in \mathcal{T}, m, n \in \mathcal{F}, mn \in MN \quad (37)$$

$$\begin{cases} \left(\pi^b_{m,t} - \pi^b_{n,t}\right)\cdot\left(f^+_{mn,t} - f^-_{mn,t}\right) \ge \pi_{n,t} - \pi_{m,t} + \left(f^+_{mn,t} - f^-_{mn,t} + 1\right)\cdot\left(\pi^{min}_{m,t} - \pi^{max}_{n,t}\right) \\ \left(\pi^b_{m,t} - \pi^b_{n,t}\right)\cdot\left(f^+_{mn,t} - f^-_{mn,t}\right) \ge \pi_{m,t} - \pi_{n,t} + \left(f^+_{mn,t} - f^-_{mn,t} - 1\right)\cdot\left(\pi^{max}_{m,t} - \pi^{min}_{n,t}\right) \\ \left(\pi^b_{m,t} - \pi^b_{n,t}\right)\cdot\left(f^+_{mn,t} - f^-_{mn,t}\right) \ge \pi_{n,t} - \pi_{m,t} + \left(f^+_{mn,t} - f^-_{mn,t} + 1\right)\cdot\left(\pi^{min}_{m,t} - \pi^{max}_{n,t}\right) \\ \left(\pi^b_{m,t} - \pi^b_{n,t}\right)\cdot\left(f^+_{mn,t} - f^-_{mn,t}\right) \ge \pi_{m,t} - \pi_{n,t} + \left(f^+_{mn,t} - f^-_{mn,t} - 1\right)\cdot\left(\pi^{max}_{m,t} - \pi^{min}_{n,t}\right) \end{cases} \quad t \in \mathcal{T}, m, n \in \mathcal{F}, mn \in MN \quad (38)$$

$$\begin{cases} GL^b_{mn,t} = \overline{GL^b_{mn,t,0}} + \sum_{r=1}^{h}\delta_r \\ y = \bar{y}_0 + \sum_{r=1}^{h}\frac{\bar{y}_r - \bar{y}_{r-1}}{GL^b_{mn,t,r} - GL^b_{mn,t,r-1}}\delta_r \\ \left(\overline{GL^b_{mn,t,r}} - \overline{GL^b_{mn,t,r-1}}\right)z_{r+1} \le \delta_r;\ r \in \{1, 2, \ldots, h-1\} \\ \delta_r \le \left(\overline{GL^b_{mn,t,r}} - \overline{GL^b_{mn,t,r-1}}\right)z_r;\ r \in \{1, 2, \ldots, h\} \end{cases} \quad t \in \mathcal{T}, mn \in MN. \quad (39)$$

B. Security Evaluation Model

As described in Section III-B, the last step of the vulnerable component identification process is to design a proper approach to quantify effects of vulnerable components failures. Specifically, the co-optimization model (8)-(39) derives unit commitment and generation dispatch solutions for the interdependent system under normal operation. However, when vulnerable components are out of service, imbalance of supply-demand in power system and/or gas network could happen. To this end, the MILP-based security evaluation model is used in this paper to quantify the influence on the interdependent system in terms of total supply-demand imbalance when identified vulnerable components are out of service. That is, the total supply-demand imbalance is calculated after the selected vulnerable components are out of service for the entire scheduling horizon to assess their impacts on the interdependent system. This process can be executed multiple times by including the top identified vulnerable components successively, i.e., one run with only the top 1 vulnerable component out of service for the entire scheduling horizon, and another run with the top 2 vulnerable components out of service for the entire scheduling horizon. This model is used to quantitively evaluate effectiveness of the proposed vulnerable component identification method, i.e., components inducing larger supply-demand imbalance after failures are more vulnerable.

- *Objective:* The objective of security evaluation is to minimize total supply-demand imbalance for the interdependent system as in (40), with respect to the unit commitment and generation dispatch solution under normal condition. In (40), natural gas system imbalance quantity is converted to electric energy quantity (i.e., from MMBtu (million British Thermal Unit) to MW). A larger objective means a more severe supply-demand imbalance under contingencies, indicating the component is indeed more vulnerable.

$$\min \sum_{t\in\mathcal{T}}\sum_{\Delta\in\beth}\left[\begin{array}{c}\sum_{e\in\mathcal{E}}\left(v^{\Delta}_{1,e,t} + v^{\Delta}_{2,e,t}\right) \\ + \sum_{f\in\mathcal{F}}\left(v^{\Delta}_{3,f,t} + v^{\Delta}_{4,f,t}\right)\cdot \text{HHV}/\Phi\end{array}\right]. \quad (40)$$

- *Constraints for Each Contingency:* Constraints (41)-(64) include limits for the interdependent system under contingencies. Constraint (41) represents generator capacity limits. Constraint (42) represents generator corrective capability. Compared to normal operation condition, constraints (43)-(44) include slack variables representing generation-load imbalance. Constraints (45)-(47) describe DC power flow limits. Constraints (48)-(50) indicate capacity limits of gas supply and gas storage. Gas storage injection/withdrawal rate limits are described as in (51)-(52). Compared to (25), slack variables are added in (53) to represent gas supply-demand imbalance. Constraints (55)-(58) describe limits of nodal pressure, pipeline flow, as well as flow of pipeline with compressor. Constraints (59)-(62) describe linepack calculation. Natural gas consumption of gas-fired units and electricity consumption of electric-driven compressors under contingency are calculated as in (63)-(64).

$$P^{min}_g \cdot I^b_{g,t} \le P^{\Delta}_{g,t} \le P^{max}_g \cdot I^b_{g,t}; \quad g \in \mathcal{G}, t \in \mathcal{T}, \Delta \in \beth \quad (41)$$

$$-R^{down}_g \cdot I^b_{g,t} \le P^{\Delta}_{g,t} - P^b_{g,t} \le R^{up}_g \cdot I^b_{g,t}; \quad g \in \mathcal{G}, t \in \mathcal{T}, \Delta \in \beth \quad (42)$$

$$\sum_{g\in N(e)\bigcap\mathcal{G}} P^{\Delta}_{g,t} - \sum_{s(l)\in N(e)\bigcap\mathcal{L}} PL^{\Delta}_{l,t} + \sum_{r(l)\in N(e)\bigcap\mathcal{L}} PL^{\Delta}_{l,t} + v^{\Delta}_{1,e,t} - v^{\Delta}_{2,e,t} = \sum_{d\in N(e)\bigcap\mathcal{D}} P^b_{d,t} + \sum_{c\in N(e)\bigcap\mathcal{C}} P^{\Delta}_{c,t}; \quad e \in \mathcal{E}, t \in \mathcal{T}, \Delta \in \beth \quad (43)$$

$$v^{\Delta}_{1,e,t}, v^{\Delta}_{2,e,t} \ge 0; \qquad e \in \mathcal{E}, t \in \mathcal{T}, \Delta \in \beth \quad (44)$$

$$-PL^{max}_l \le PL^{\Delta}_{l,t} \le PL^{max}_l; \qquad l \in \mathcal{L}, t \in \mathcal{T}, \Delta \in \beth \quad (45)$$

$$PL^{\Delta}_{l,t} = \left(\theta^{\Delta}_{s(l)t} - \theta^{\Delta}_{r(l)t}\right)/x_l; \qquad l \in \mathcal{L}, t \in \mathcal{T}, \Delta \in \beth \quad (46)$$

$$\theta^{min}_e \le \theta^{\Delta}_{e,t} \le \theta^{max}_e;\ \theta^{\Delta}_{ref,t} = 0; \quad e \in \mathcal{E}, t \in \mathcal{T}, \Delta \in \beth \quad (47)$$

$$G^{min}_k \le G^{\Delta}_{k,t} \le G^{max}_k; \qquad k \in \mathcal{K}, t \in \mathcal{T}, \Delta \in \beth \quad (48)$$

$$E^{\Delta}_{s,t} = E^{\Delta}_{s,(t-1)} + Q^{in,\Delta}_{s,t} - Q^{out,\Delta}_{s,t}; \quad s \in \mathcal{S}, t \in \mathcal{T}, \Delta \in \beth \quad (49)$$

$$E^{min}_s \le E^{\Delta}_{s,t} \le E^{max}_s; \qquad s \in \mathcal{S}, t \in \mathcal{T}, \Delta \in \beth \quad (50)$$

$$Q^{min}_s \le Q^{in,\Delta}_{s,t} \le Q^{max}_s; \qquad s \in \mathcal{S}, t \in \mathcal{T}, \Delta \in \beth \quad (51)$$

$$Q^{min}_s \le Q^{out,\Delta}_{s,t} \le Q^{max}_s; \qquad s \in \mathcal{S}, t \in \mathcal{T}, \Delta \in \beth \quad (52)$$

$$\sum_{k\in G(f)\bigcap\mathcal{K}} G^{\Delta}_{k,t} + \sum_{s\in G(f)\bigcap\mathcal{S}} \left(Q^{out,\Delta}_{s,t} - Q^{in,\Delta}_{s,t}\right) + \sum_{mn\in G(f)\bigcap MN} \left(Q^{out,\Delta}_{mn,t} - Q^{in,\Delta}_{mn,t}\right) + v^{\Delta}_{3,f,t} - v^{\Delta}_{4,f,t} = \sum_{g\in G(f)\bigcap\mathcal{G}} G^{\Delta}_{g,t} + \sum_{w\in G(f)\bigcap\mathcal{W}} G^{b}_{w,t};$$
$$f\in\mathcal{F}, t\in\mathcal{T}, \Delta\in\mathcal{A} \quad (53)$$

$$v^{\Delta}_{3,f,t}, v^{\Delta}_{4,f,t} \geq 0; \qquad f\in\mathcal{F}, t\in\mathcal{T}, \Delta\in\mathcal{A} \quad (54)$$

$$GL^{\Delta}_{mn,t} = \mathrm{sgn}\left(\pi^{\Delta}_{m,t}, \pi^{\Delta}_{n,t}\right)\cdot K_{mn}\cdot\sqrt{\left|\pi^{\Delta}_{m,t} - \pi^{\Delta}_{n,t}\right|}; \quad t\in\mathcal{T}, m, n\in\mathcal{F}, mn\in MN, \Delta\in\mathcal{A} \quad (55)$$

$$\mathrm{sgn}\left(\pi^{\Delta}_{m,t}, \pi^{\Delta}_{n,t}\right) = \begin{cases} 1, & \pi^{\Delta}_{m,t} \geq \pi^{\Delta}_{n,t} \\ -1, & \pi^{\Delta}_{m,t} < \pi^{\Delta}_{n,t} \end{cases} \quad m, n\in\mathcal{F},\ t\in\mathcal{T}, \Delta\in\mathcal{A} \quad (56)$$

$$\pi^{min}_{m} \leq \pi^{\Delta}_{m,t} \leq \pi^{max}_{m}; \qquad m\in\mathcal{F}, t\in\mathcal{T}, \Delta\in\mathcal{A} \quad (57)$$

$$\pi^{\Delta}_{m,t} \leq \tau_c^2\cdot\pi^{\Delta}_{n,t}; \qquad m, n\in\mathcal{F}, t\in\mathcal{T}, \Delta\in\mathcal{A} \quad (58)$$

$$E^{\Delta}_{mn,t} = L_{mn}\cdot\rho^{\Delta}_{mn,t}; \qquad mn\in MN, t\in\mathcal{T}, \Delta\in\mathcal{A} \quad (59)$$

$$\rho^{\Delta}_{mn,t} = (\rho^{\Delta}_{m,t} + \rho^{\Delta}_{n,t})/2;\ \pi^{\Delta}_{m,t} = \rho^{\Delta 2}_{m,t}\ m, n\in\mathcal{F},\ t\in\mathcal{T}, \Delta\in\mathcal{A} \quad (60)$$

$$E^{\Delta}_{mn,t} = E^{\Delta}_{mn,(t-1)} + Q^{in,\Delta}_{mn,t} - Q^{out,\Delta}_{mn,t}; \quad mn\in MN, t\in\mathcal{T}, \Delta\in\mathcal{A} \quad (61)$$

$$GL^{\Delta}_{mn,t} = (Q^{in,\Delta}_{mn,t} + Q^{out,\Delta}_{mn,t})/2;\ mn\in MN, t\in\mathcal{T}, \Delta\in\mathcal{A} \quad (62)$$

$$G^{\Delta}_{g,t} = \frac{\left[\left(F^{c}_{g}\left(P^{\Delta}_{g,t}\right)\cdot I^{b}_{g,t}\right) + su^{b}_{g,t} + sd^{b}_{g,t}\right]}{\mathrm{HHV}}; \quad g\in\mathcal{GU}, t\in\mathcal{T}, \Delta\in\mathcal{A} \quad (63)$$

$$P^{\Delta}_{c,t} = \left(1 - e^{com}_{c}\right)\cdot Q^{\Delta}_{c,t}\cdot\mathrm{HHV}/\Phi;\ \mathrm{c}\in\mathcal{C},\ t\in\mathcal{T}, \Delta\in\mathcal{A}. \quad (64)$$

V. Numerical Example

A 6-bus electricity/7-node gas system and a modified IEEE 118-bus electricity/20-node gas system are used to test effectiveness of the proposed vulnerability identification and security evaluation methods. The 6-bus electricity/7-node gas system is first used to show advantages of the proposed method in identifying and ranking vulnerable components. Then, effectiveness of the proposed method under different operation conditions is illustrated by modifying system parameters such as generation, load, as well as power system and gas system topology. The modified IEEE 118-bus electricity/20-node gas system is used to show advantages of the proposed method by comparing identified vulnerable components for interdependent system and independent power system/natural gas system. The proposed co-optimization and security evaluation models are implemented in MATLAB and solved by GUROBI with YALMIP.

A. The 6-Bus Electricity/7-Node Gas System

1) Identification of Vulnerable Components: The 6-bus electricity/7-node gas system is shown in Fig. 1, and the detailed data can be found in [40]. For the traditional detailed topological model, 28 vertices are included to describe this interdependent system, while the proposed model only includes 16 vertices, which could reduce the topological scale and computational burden. The 24-hour co-optimization model is used to obtain flow information. Values of vulnerability index R for Hour 8 and Hour 20 are listed in Table I to rank and identify vulnerable components. The betweenness centrality (BC) [24] and closeness centrality (CC) [25] are also included in Table I for comparison.

TABLE I
Vulnerability Ranking of Components for the 6-Bus Electricity/7-Node Natural Gas System

Rank of R	Infrastructure ID					
	Hour 8			Hour 20		
	Proposed(R)	BC	CC	Proposed(R)	BC	CC
1	V2(0.8074)	C1	C1	V2(0.8987)	C1	C1
2	V1(0.5987)	N2	N2	V4(0.5461)	N2	N2
3	V4(0.4614)	V4	V4	N2(0.5098)	V4	V4
4	N2(0.4559)	N5	N1	V6(0.4840)	N5	V6
5	V3(0.3836)	N4	V2	V3(0.4568)	V6	V3
6	N5(0.2738)	N1	G5	N5(0.4111)	V3	V2
7	V6(0.2550)	V3	V3	C1(0.2893)	N4	N5
8	C1(0.2483)	G5	N5	V1(0.2534)	G4	V5
9	N1(0.2196)	V2	N4	N1(0.2483)	N3	N1
10	N6(0.1405)	V5	V5	N3(0.1376)	N1	G5
11	N4(0.0792)	V6	V1	N4(0.0793)	V2	G4
12	G5(0.0659)	G4	V6	N6(0.0621)	V5	N4
13	N3(0.0656)	N7	N7	V5(0.0445)	G5	N3
14	N7(0.0441)	N6	N6	N7(0.0338)	N7	V1
15	V5(0.0382)	N3	N3	G4(0.0280)	N6	N6
16	G4(0.0100)	V1	G4	G5(0.0273)	V1	N7

In Table I, component with a larger R value means that failure of this component will have a more severe impact on the interdependent system, thus it is ranked higher in the vulnerable component list. According to result of the 24-hour co-optimization problem, G1, G2, and G5 are ON at Hour 8, while G1, G2, G4, and G5 are ON at Hour 20. That is, topologies of the interdependent system at Hour 8 and Hour 20 are different. As shown in Table I, vulnerability rank of components at Hour 8 and Hour 20 are different because of their different topology and flow patterns. We can conclude that the proposed dynamic vulnerability index can accurately recognize vulnerability of components with changes of unit commitment status and generation dispatch.

On the other hand, BC and CC only consider topology information of the interdependent system, thus vulnerable components identified via these two methods may not be accurate. For instance, C1 is identified as the most vulnerable component at both hours via BC and CC, while V2 is the most vulnerable component for the proposed method. This is because V2 is not only topologically important, but also a key power flow exchange channel for the interdependent system. Indeed, if V2 is out of service, output of G2 cannot be delivered to loads and D1 cannot be supplied. Moreover, electric power delivered to V4 may also be impacted and further C1 will be impacted.

To further show effectiveness of the proposed method, geodesic vulnerability [11] is used to quantify effects on the interdependent system after vulnerable components are out of service, as shown in Fig. 2. This index is used to measure the performance of a system under successive contingencies: the faster the index value decreases, the more vulnerable the

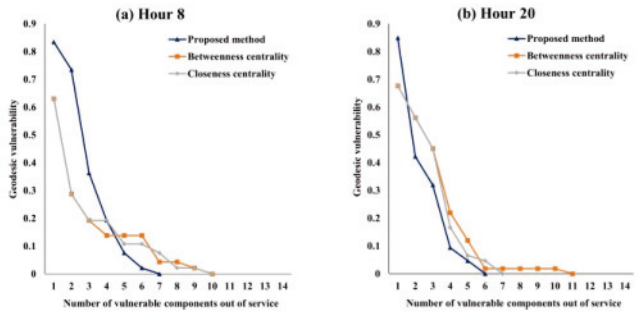

Fig. 2. Geodesic vulnerability of the 6-bus electricity/7-node gas system.

components. For the interdependent system, if one component is on contingency, other components directly connected to it may also not work and should be excluded when calculating geodesic vulnerability.

As shown in Fig. 2, the proposed method performs better than BC and CC at both hours. At Hour 8, the geodesic vulnerability becomes 0 when the top 7 vulnerable components derived from the proposed method are out of service, while the top 10 vulnerable components are needed for both BC and CC methods. At Hour 20, the proposed method only needs the top 6 vulnerable components to reach 0 geodesic vulnerability, and geodesic vulnerability value of the proposed method drops much faster when the first 2 components are out of service. In turn, we can conclude that vulnerable components identified by the proposed method is more effective than BC and CC methods.

The proposed security evaluation method is further used to calculate electricity and gas supply-demand imbalance after the top 6 vulnerable components are out of service successively, to quantify their impacts on the interdependent system. The results for hour 8 are shown in Table II for the detailed discussion. Compared with BC and CC, failures of top vulnerable components identified from the proposed method result in higher electricity and gas supply-demand imbalance, indicating that vulnerable components identified by the proposed method are indeed critical. Indeed, the entire electricity system will be out of service after the top 5 vulnerable components identified from the proposed method fail (i.e., all committed generators connected to vertices V1, V2, and V3 are isolated, while G3 and G4 connected to vertices V5 and V6 are not committed), while the top 6 vulnerable components for CC method need to be out to achieve the similar effect. In addition, for BC method, although the gas supply-demand imbalance increases fast because of gas system's topological characteristics, electricity supply-demand imbalance increases much slower than the proposed method. Therefore, it clearly shows that, by simultaneously considering topological and functional vulnerabilities, the proposed method is more effective than BC and CC methods in identifying vulnerable components.

2) Comparison of Different Operation Conditions: As analyzed above, results of component vulnerabilities are different under different topologies. To this end, the system is modified to study impacts of operation conditions on vulnerable component identification results. The operation condition of Section V-A1 is denoted as the base operation condition and

TABLE II
SUPPLY-DEMAND IMBALANCE ANALYSIS FOR THE 6-BUS ELECTRICITY/7-NODE GAS SYSTEM

# of Component failures		1	2	3	4	5	6
Component ID	Proposed	V2	V1	V4	N2	V3	N5
	BC	C1	N2	V4	N5	N4	N1
	CC	C1	N2	V4	N1	V2	G5
Electricity supply + demand imbalance /MWh	Proposed	68.89 +0.00	268.89 +150.00	268.89 +150.00	298.89 +150.00	298.89 +150.00	298.89+ 150.00
	BC	0.00 +0.00	0.00 +0.00	123.89 +0.00	123.89 +0.00	225.10 +69.93	298.89 +143.72
	CC	0.00 +0.00	0.00 +0.00	123.89 +0.00	225.10 +69.93	298.89 +143.72	298.89 +150.00
Gas supply + demand imbalance /MMBtu	Proposed	0.00 +0.00	0.00 +0.00	0.00 +0.00	3,963.63 +0.00	3,963.63 +0.00	6,190.68 + 2,000.00
	BC	0.00 +0.00	3,963.63 +0.00	3,963.63 +0.00	6190.68 + 2,000.00	6,190.68 + 2,000.00	6,190.68 + 2,000.00
	CC	0.00 +0.00	3,963.63 +0.00	3,963.63 +0.00	3,963.63 +0.00	3,963.63 +0.00	3,963.63 +0.00

TABLE III
VULNERABILITY RANKING OF COMPONENTS AGAINST DIFFERENT OPERATION CONDITIONS

Rank of *R*	Hour 8				Hour20			
	S1	S2	S3	S4	S1	S2	S3	S4
1	V2	V3	V2	N5	V2	V3	V2	N5
2	V1	C1	V1	N1	V4	N2	V6	N1
3	V4	N2	V6	N7	N2	V6	V1	N3
4	N2	V4	V3	N3	V6	V2	V3	N7
5	V3	V1	V5	N2	V3	C1	V5	N2
6	N5	V2	N2	N6	N5	V4	N2	N6
7	V6	N1	N5	N4	C1	N1	N5	N4
8	C1	N5	N6	V2	V1	V1	N1	V2
9	N1	V6	N1	V1	N1	N5	N3	V6
10	N6	N4	C1	V3	N3	N3	N6	V3
11	N4	G5	V4	V6	N4	N4	V4	V1
12	G5	N6	N3	V4	N6	G5	C1	V4
13	N3	N7	N4	G5	V5	V5	N7	C1
14	N7	N3	G5	C1	N7	N6	N4	G5
15	V5	V5	N7	V5	G4	G4	G4	G4
16	G4	G4	G4	G4	G5	N7	G5	V5

shown as S1 in Table III. Electrical demands of D2 and D3 as well as capacities and ramping rates of G2 and G5 are interchanged to build S2 in Table III. For S3, four transmission lines V1-V5, V2-V6, V3-V5, and V2-V5 are added to increase topological complexity of the power system. Similarly, seven pipelines N1-N3, N1-N5, N2-N3, N4-N5, N4-N6, N6-N7, and N5-N7 are added in S4 to increase natural gas system topological complexity.

Table III shows vulnerability rank of components under different operation conditions. It clearly shows that when topologies are same, vulnerabilities of components are influenced by generator/load parameters which impact flow pattern characteristics. Compared to S1, in S2, V3 replaces V2 and becomes the most vulnerable component, because capacity of G2 is larger than G5 and electrical demand of D3 is higher than D2. Moreover, we find that component vulnerability also depends on topological complexity. In S3, vulnerability ranks of power system components increase when power system complexity increases, i.e., the top 5 vulnerable components

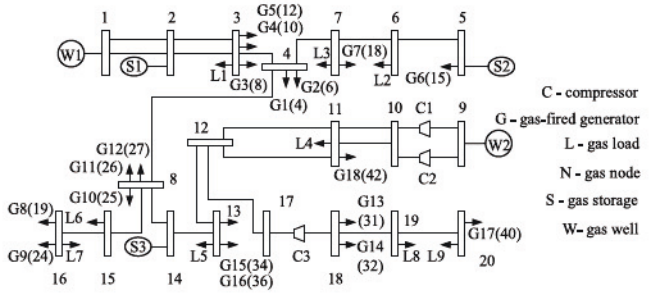

Fig. 3. The 20-node natural gas system.

are all from power system at both Hour 8 and Hour 20; in comparison, in S4, components from gas system have higher vulnerability ranks, when the gas system topological complexity is increased.

B. The Modified IEEE 118-Bus Electricity/20-Node Gas System

The modified 118-bus electricity/20-node gas system includes 18 gas-fired generators and 3 electric-driven compressors. C1 and C2 are connected to bus 9 of the power system, and C3 is connected to electric bus 17 of the power system. Fig. 3 shows the 20-node natural gas system together with the interconnection information of the gas-fired units. Other data can be referred to from [40]. The detailed topology model includes 300 vertices to describe this interdependent system, while the proposed model only includes 159 vertices, which would significantly reduce topological scale and consequently computational burden.

Table IV shows vulnerable component ranks calculated by the proposed approach as well as the BC and CC. The proposed security evaluation method is also used to calculate electricity and gas supply-demand imbalance after the vulnerable components are out of service successively, to quantify their impacts on the interdependent system. In Table IV, IDs of components with prefix N or C indicate assets of the natural gas system, while other IDs are for power system components.

As aforementioned, topological complexity will influence vulnerability rankings of individual components. To this end, in this interdependent system, because the scale of natural gas network is much smaller than the power grid, the top 30 vulnerable components are mostly from the power system. In comparison, vulnerable components identified via the proposed method include more gas system components than BC and CC, for the reason that the proposed vulnerability index considers both topological and functional vulnerabilities simultaneously. Electricity and gas supply-demand imbalance are calculated when different sets of vulnerable components are out of service (i.e., top 5, 10, 15, 20, 25, and 30). Compared with BC and CC, components failures identified from the proposed method result in more extensive electricity and gas supply-demand imbalance, indicating that vulnerable components identified by our method are indeed critical.

TABLE IV
VULNERABILITY ANALYSIS FOR THE MODIFIED IEEE 118-BUS ELECTRICITY/20-NODE GAS SYSTEM

# of Component failures		5	10	15	20	25	30
Component ID	Proposed	80,81,N3 49,N4	69,N1, N8,100, 77	N2,N15, 54,N16, 94	92,59,96, 75,17	N7,56, 47,15,70	12,66,65, 62,60
	BC	80,49,69, 77,38	30,65, 100,C3, 17	N18,70, 68,8,24	31,37,15, 98,99	82,23,42, N8,32	N12,12, G13,66, 40
	CC	38,65,69, 68,30	49,17,80, 37,C3	77,31,70, 42,66	81,75,32, 40,N18	24,23,15, N12,G13	47,26,33, 113,34
Electricity supply + demand imbalance /MWh	Proposed	249.02 +57.71	1,256.82 +298.46	1,418.94 +328.59	1,771.75 +359.64	1,851.75 +359.64	2,445.59 +822.27
	BC	1,118.87 +137.71	1,118.87 +389.71	1,293.87 +426.81	1,329.93 +526.81	1,527.70 +526.81	1,793.56 +737.44
	CC	269.92 +332.00	918.87 +389.71	1,137.65 +600.34	1,137.65 +600.34	1,179.94 +600.34	1,412.60 +700.34
Gas supply + demand imbalance /MMBtu	Proposed	3,402.94 +0.00	4,513.03 +0.00	15,392.7 6+0.00	15,392.7 6+0.00	18,294.2 7+0.00	18,294.2 7+0.00
	BC	0.00 +0.00	0.00 +0.00	0.00 +0.00	0.00 +0.00	1,110.10 +0.00	1,110.10 +0.00
	CC	0.00 +0.00	0.00 +0.00	0.00 +0.00	0.00 +0.00	0.00 +0.00	0.00 +0.00

TABLE V
VULNERABILITY COMPONENTS OF INDEPENDENT AND INTERDEPENDENT SYSTEMS

Rank of vulnerable components	Infrastructure ID		Rank of vulnerable components	Infrastructure ID	
	Natural gas system	Power system		Natural gas system	Power system
1	N4	80	13	N10	96
2	N8	81	14	N6	56
3	N3	68	15	N17	47
4	N15	49	16	C1	70
5	N2	69	17	C2	66
6	N7	100	18	C3	62
7	N14	77	19	N9	65
8	N1	54	20	N18	17
9	N13	94	21	N19	60
10	N11	59	22	N5	103
11	N12	92	23	N20	55
12	N16	75	24	/	12

Moreover, we apply the proposed vulnerable component identification method to evaluate the natural gas system and power system separately, while neglecting their interdependence. The results are shown in Table V. Comparing with Table IV, we can find that vulnerable components of interdependent system are not a simple combination of those identified from separate systems. For instance, the top 3 vulnerable gas components of the independent system are N4, N8, and N3, while are N3, N4, and N1 for the interdependent system.

VI. CONCLUSION

Vulnerable component identification plays an important role in secure operation of interdependent systems such as natural gas-electricity system. This paper constructs a topological model of the interdependent system and discusses a novel vulnerable component identification method. Effectiveness of the proposed method is verified by calculating electricity and gas supply-demand imbalance of the interdependent system

when the identified vulnerable components are out of service. The following observations are obtained from numerical results:

(i) The proposed vulnerability index is dynamical, which can reflect actual operation status of interdependent systems (i.e., topology as well as generator/load parameters);

(ii) By simultaneously considering topological and functional vulnerability, vulnerable components identified by the proposed method is more reasonable and effective than existing approaches such as BC and CC methods;

(iii) For the interdependent system, vulnerable components depend on topological complexity of the system, which are also different from those identified from separate systems;

(iv) The proposed topological model is more accurate than traditional model, and can reduce modeling scale than detailed topological model while preserve all characteristics.

REFERENCES

[1] R. Holden, D. V. Val, R. Burkhard, and S. Nodwell, "A network flow model for interdependent infrastructures at the local scale," *Safety Sci.*, vol. 53, pp. 51–60, Mar. 2013.

[2] C. Heracleous, P. Kolios, C. G. Panayiotou, G. Ellinas, and M. M. Polycarpou, "Hybrid systems modeling for critical infrastructures interdependency analysis," *Reliab. Eng. Syst. Safety*, vol. 165, pp. 89–101, Sep. 2017.

[3] M. Ouyang, L. Hong, Z.-J. Mao, M.-H. Yu, and F. Qi, "A methodological approach to analyze vulnerability of interdependent infrastructures," *Simulat. Model. Pract. Theory*, vol. 17, no. 5, pp. 817–828, 2009.

[4] *Natural Gas Monthly*. Accessed: Aug. 2019. [Online]. Available: https://www.eia.gov/naturalgas/monthly/pdf/ngm_all.pdf

[5] C. He, L. Wu, T. Liu, and M. Shahidehpour, "Robust co-optimization scheduling of electricity and natural gas systems via ADMM," *IEEE Trans. Sustain. Energy*, vol. 8, no. 2, pp. 658–670, Apr. 2017.

[6] C. He, L. Wu, T. Liu, and Z. Bie, "Robust co-optimization planning of interdependent electricity and natural gas systems with a joint N-1 and probabilistic reliability criterion," *IEEE Trans. Power Syst.*, vol. 33, no. 2, pp. 2140–2154, Mar. 2018.

[7] C. Liu, M. Shahidehpour, and J. Wang, "Coordinated scheduling of electricity and natural gas infrastructures with a transient model for natural gas flow," *Chaos*, vol. 21, no. 2, 2011, Art. no. 025102.

[8] S. B. Dokic and N. L. Rajakovic, "Security modelling of integrated gas and electrical power systems by analyzing critical situations and potentials for performance optimization," *Energy*, vol. 184, pp. 141–150, Oct. 2019.

[9] M. Ouyang, "Review on modeling and simulation of interdependent critical infrastructure systems," *Reliab. Eng. Syst. Safety*, vol. 121, pp. 43–60, Jan. 2014.

[10] B. Wang, S. Wan, X. Zhang, and K.-K. R. Choo, "A novel index for assessing the robustness of integrated electrical network and a natural gas network," *IEEE Access*, vol. 6, pp. 40400–40410, 2018.

[11] J. Beyza, E. Garcia-Paricio, and J. M. Yusta, "Ranking critical assets in interdependent energy transmission networks," *Elect. Power Syst. Res.*, vol. 172, pp. 242–252, Jul. 2019.

[12] G. J. Correa and J. M. Yusta, "Geodesic vulnerability index for contingency analysis in electric infrastructures," in *Proc. VII Symp. Power Qual. (SICEL)*, Nov. 2013, pp. 1–7.

[13] P. Crucitti, V. Latora, and M. Marchiori, "Model for cascading failures in complex networks," *Phys. Rev. E, Stat. Phys. Plasmas Fluids Relat. Interdiscip. Top*, vol. 69, no. 4, 2004, Art. no. 045104.

[14] J. Beyza and J. M. Yusta, "Robustness assessment of the expansion of coupled electric power and natural gas networks under cascading failures," *IET Gen. Transm. Distrib.*, vol. 12, no. 21, pp. 5753–5760, 2018.

[15] P. Hines, E. Cotilla-Sanchez, and S. Blumsack, "Do topological models provide good information about electricity infrastructure vulnerability," *Chaos*, vol. 20, no. 3, 2010, Art. no. 033122.

[16] B. C. Erdener, K. A. Pambour, R. B. Lavin, and B. Dengiz, "An integrated simulation model for analysing electricity and gas systems," *Int. J. Elect. Power Energy Syst.*, vol. 61, pp. 410–420, Oct. 2014.

[17] X. Wei, J. Zhao, T. Huang, and E. Bompard, "A novel cascading faults graph based transmission network vulnerability assessment method," *IEEE Trans. Power App. Syst.*, vol. 33, no. 3, pp. 2995–3000, May 2018.

[18] A. M. Haidar, A. Mohamed, and A. Hussain, "Vulnerability assessment of a large sized power system using a new index based on power system loss," *Eur. J. Sci. Res.*, vol. 17, no. 1, pp. 61–72, 2007.

[19] S. P. Dwivedi and R. S. Singh, "Error-tolerant graph matching using node contraction," *Pattern Recognit. Lett.*, vol. 116, pp. 58–64, Dec. 2018.

[20] S. Gupta, F. Kazi, S. Wagh, and N. Singh, "Analysis and prediction of vulnerability in smart power transmission system: A geometrical approach," *Int. J. Elect. Power Energy Syst.*, vol. 94, pp. 77–87. Jan. 2018.

[21] B. Zhao, A. J. Conejo, and R. Sioshansi, "Coordinated expansion planning of natural gas and electric power systems," *IEEE Trans. Power Syst.*, vol. 33, no. 3, pp. 3064–3075, May 2018.

[22] J. A. Kersulis, I. A. Hiskens, C. Coffrin, and D. K. Molzahn, "Topological graph metrics for detecting grid anomalies and improving algorithms," in *Proc. IEEE Power Syst. Comput. Conf.*, 2018, Art. no. 18073259.

[23] S. Chanda and A. K. Srivastava, "Defining and enabling resiliency of electric distribution systems with multiple microgrids," *IEEE Trans. Smart Grid*, vol. 7, no. 6, pp. 2859–2868, Nov. 2016.

[24] Y. Cai, Y. Cao, Y. Li, T. Huang, and B. Zhou, "Cascading failure analysis considering interaction between power grids and communication networks," *IEEE Trans. Smart Grid*, vol. 7, no. 1, pp. 530–538, Jan. 2016.

[25] B. Wei and Y. Deng, "A cluster-growing dimension of complex networks: From the view of node closeness centrality," *Phys. A, Stat. Mech. Appl.*, vol. 522, pp. 80–87. May 2019.

[26] D. Chen, L. Lü, M.-S. Shang, Y.-C. Zhang, and T. Zhou, "Identifying influential nodes in complex networks," *Phys. A, Stat. Mech. Appl.*, vol. 391, no. 4, pp. 1777–1787, 2012.

[27] W. Y. Ng, "Generalized generation distribution factors for power system security evaluations," *IEEE Trans. Power App. Syst.*, vol. PAS-100, no. 3, pp. 1001–1005, Mar. 1981.

[28] H. Zhong, Q. Xia, Y. Wang, and C. Kang, "Dynamic economic dispatch considering transmission losses using quadratically constrained quadratic program method," *IEEE Trans. Power Syst.*, vol. 28, no. 3, pp. 2232–2241, Aug. 2013.

[29] L. Yang, Y. Xu, H. Sun, and X. Zhao, "Two-stage convexification based optimal electricity-gas flow," *IEEE Trans. Smart Grid*, early access, doi: 10.1109/TSG.2019.2938553.

[30] Y. Zhang, J. Wang, B. Zeng, and Z. Hu, "Chance-constrained two-stage unit commitment under uncertain load and wind power output using bilinear benders decomposition," *IEEE Trans. Power Syst.*, vol. 32, no. 5, pp. 3637–3647, Sep. 2017.

[31] C. Zhao and Y. Guan, "Unified stochastic and robust unit commitment," *IEEE Trans. Power Syst.*, vol. 28, no. 3, pp. 3353–3361, Aug. 2013.

[32] S. An, Q. Li, and T. W. Gedra, "Natural gas and electricity optimal power flow," in *Proc. IEEE PES Transm. Distrib. Conf. Expo.*, vol. 1, 2003, pp. 138–143.

[33] Q. Zeng, J. Fang, J. Li, and Z. Chen, "Steady-state analysis of the integrated natural gas and electric power system with bi-directional energy conversion," *Appl. Energy*, vol. 184, pp. 1483–1492, Dec. 2016.

[34] J. H. Zheng, Q. H. Wu, and Z. X. Jing, "Coordinated scheduling strategy to optimize conflicting benefits for daily operation of integrated electricity and gas networks," *Appl. Energy*, vol. 192, pp. 370–381, Apr. 2017.

[35] S. Wu, R. Z. Ríos-Mercado, E. A. Boyd, and L. R. Scott, "Model relaxations for the fuel cost minimization of steady-state gas pipeline networks," *Math. Comput. Model.*, vol. 31, nos. 2–3, pp. 197–220, 2000.

[36] E. S. Menon, *Gas Pipeline Hydraulics*. Boca Raton, FL, USA: CRC Press, 2005.

[37] B. Gei, A. Martin, A. Morsi, and L. Schewe, "Using piecewise linear functions for solving MINLPs," in *Mixed Integer Nonlinear Programming*, New York, NY, USA: Springer, 2012, pp. 287–314. [Online]. Available: https://doi.org/10.1007/978-1-4614-1927-3_10

[38] G. Mccormick, "Computability of global solutions to factorable nonconvex programs: Part I—Convex underestimating problems," *Math. Program.*, vol. 10, no. 1, pp. 147–175, 1976.

[39] T. Ding, R. Bo, W. Gu, and H. Sun, "Big-M based MIQP method for economic dispatch with disjoint prohibited zones," *IEEE Trans. Power Syst.*, vol. 29, no. 2, pp. 976–977, Mar. 2014.

[40] *Test System Data*. Accessed: Sep. 2019. [Online] Available: https://sites.google.com/site/leiwupes/data/IGE_data.xlsx

Lu Nan (Student Member, IEEE) received the B.S. degree in electrical engineering from Sichuan University, Chengdu, China, in 2016, where she is currently pursuing the Ph.D. degree. She was a visiting Ph.D. student with the Stevens Institute of Technology, Hoboken, NJ, USA, from 2018 to 2019. Her research interests include vulnerability analysis and optimal operation of power grids.

Lei Wu (Senior Member, IEEE) received the B.S. degree in electrical engineering and the M.S. degree in systems engineering from Xian Jiaotong University, Xi'an, China, in 2001 and 2004, respectively, and the Ph.D. degree in electrical engineering from the Illinois Institute of Technology, Chicago, IL, USA, in 2008. He was a Senior Research Associate with the Robert W. Galvin Center for Electricity Innovation, IIT from 2008 to 2010. He worked as a summer Visiting Faculty with NYISO in 2012. He was a Professor with the Electrical and Computer Engineering Department, Clarkson University, Potsdam, NY, USA, till 2018. He is currently an Associate Professor with the Electrical and Computer Engineering Department, Stevens Institute of Technology, Hoboken, NJ, USA. His research interests include power systems operation and planning, energy economics, and community resilience microgrid.

Tianqi Liu (Senior Member, IEEE) received the B.S. and M.S. degrees in electrical engineering from Sichuan University, Chengdu, China, in 1982 and 1986, respectively, and the Ph.D. degree in electrical engineering from Chongqing University, Chongqing, China, in 1996. She is currently a Professor with the College of Electrical Engineering, Sichuan University. Her main research interests are power system analysis and stability control, HVDC, optimal operation, dynamic security analysis, dynamic state estimation, and load forecast.

Yikui Liu (Student Member, IEEE) received the B.S. degree in electrical engineering and automation from the Nanjing Institute of Technology, China, in 2012, and the M.S. degree in power system and automation from Sichuan University, China, in 2015. He is currently pursuing the Ph.D. degree with the Electrical and Computer Engineering Department, Stevens Institute of Technology, USA. His current research interests are power market and OPF in distribution system.

Chuan He (Member, IEEE) received the B.S., M.S., and Ph.D. degrees in electrical engineering from Sichuan University, Chengdu, China, in 2011, 2014, and 2018, respectively. He is currently an Associate Professor with the College of Electrical Engineering, Sichuan University. He was a visiting Ph.D. student with Clarkson University, Potsdam, NY, USA, from 2015 to 2017. His research interests include robust optimization on power system operation and planning with renewable energy.